A R C H I V E S O F M E T A L L U R G Y A N D M A T E R I A L S
Volume 60 2015 Issue 2
DOI: 10.1515/amm-2015-0115

G. JEONG*, J. PARK*, S. NAM*, S.-E. SHIN**, J. SHIN**, D. BAE**, H. CHOI*,♯

THE EFFECT OF GRAIN SIZE ON THE MECHANICAL PROPERTIES OF ALUMINUM

WPŁYW WIELKOŚCI ZIARNA NA WŁAŚCIWOŚCI MECHANICZNE ALUMINIUM

Although many studies have focused on the unique plastic deformation behavior of nanocrystalline aluminum (e.g., the positive deviation from Hall-Petch relation, the unusual yield-drop phenomenon in tensile mode, etc.), the data reported by different research groups are inconsistent with each other, possibly because of different fabrication processes. In this study, aluminum samples with a wide grain-size spectrum – from a few micrometers down to 100 nanometers – are manufactured by powder metallurgy. The grain size was measured by X-ray diffraction analysis and transmission electron microscope observation. Furthermore, the tensile behavior, which varied according to a grain size, is discussed with a comparison of the theoretical models.

Keywords: Nanocrystalline aluminum, Grain size, Tensile behavior, Microstructure, Mechanical properties

1. Introduction

The dependency of the deformation mechanism of metals on grain size has been extensively investigated over the past few decades [1-24]. In particular, nanocrystalline (NC, grain size below 100nm) metals have recently been investigated to demonstrate significantly different deformation behaviors from that of ultrafine crystalline (UFC, grain size in the range from 100nm to 500nm) or microcrystalline (MC, grain size above 500nm) metals [2-24].

For UFC and MC metals, as the grain size decreases, yield stress could increase according to the Hall-Petch relationship [2-4]; when the grain size is relatively large, greater stresses can be concentrated near the adjacent grains due to the presence of multiple pile-up dislocations, leading to decreased yield stress. On the other hand, as the grain size is further reduced into the NC regime, the plastic deformation, by means of intragranular slip by lattice dislocations, begins to lose its significance, providing yield stress that deviated from the Hall-Petch relationship [5-10]. An absence of forest dislocations within nano-sized grains during deformation can lead to specific deformation mechanisms. For example, an NC nickel has demonstrated the movement of either perfect or partial dislocations as well as the formation of deformation twins that initiated from the grain boundaries [11], and electrodeposited NC copper has exhibited grain-boundary mediated diffusion creep [12]. Furthermore, limited intragranular slip, enhanced atomic shuffling, and stress-assisted free volume migration have been reported [9, 13-15]. Molecular dynamic (MD) simulations have also shown additional intragranular slip characterized by the emission of partial dislocations [16, 17].

For NC aluminum with high stacking-fault energy (SFE), Haque et al. [18] investigated sputter-deposited aluminum films with mean grain sizes of 11 and 22 nm, showing a reverse Hall-Petch relationship due to the activities of grain-boundary mediated mass flow [19, 20]. In addition, it has also been experimentally observed that partial dislocations emitted from grain boundaries can travel the grain interior for thin films [9] and powders produced by cryogenic ball milling [13, 21]. However, an experimental study using an extruded NC aluminum bulk has reported results that are completely opposite to a positive deviation from the Hall-Petch relation [22]. Recently, UFC aluminum fabricated by accumulative roll bonding has exhibited limited uniform elongation and unexpected yield-drop-like phenomenon [23], while it has not been observed in UFC aluminum having undergone powder metallurgy with similar grain sizes [24].

These inconsistent deformation behaviors may originate from abnormal microstructural characteristics or artifacts, which originate from fabrication methods. Specimens, in the form of a thin film or powder, might not provide a reliable insight, especially under tensile modes, possibly due to the restricted specimen size and the presence of unexpected artifacts [13, 19, 20]. Likewise, specimens prepared via severe plastic deformation (SPD) routes possess high fraction of high-angle grain boundaries, which might affect deformation behaviors as well. It is, therefore, a demanding task to fabricate porosity/artifact-free bulk specimens with a wide grain-size spectrum (from a few micrometers down to 100 nanometers)

* SCHOOL OF ADVANCED MATERIALS ENGINEERING, KOOKMIN UNIVERSITY, SEOUL, REPUBLIC OF KOREA
** SCHOOL OF ADVANCED MATERIALS ENGINEERING, YONSEI UNIVERSITY, SEOUL, REPUBLIC OF KOREA
♯ Corresponding author: hyunjoo@kookmin.ac.kr

using the same fabrication route and to evaluate their mechanical properties. In this study, we produce porosity/artifact-free bulk aluminums with grain sizes ranging from ~2.2 μm to 100 nm, and they are tested using conventional mechanical testing methods. Grain sizes were measured by X-ray diffraction (XRD) analysis and transmission electron microscope (TEM) observations. The experimentally measured tensile behaviors of the specimens are compared with the previously reported data and theoretical models.

2. Experimental procedure

Aluminum sheets, with a wide grain size spectrum from a few micrometers down to 100 nanometers, were fabricated by hot rolling ball-milled powder. A ball-milling process using a planetary mill (TMC Co. Ltd., Pulverisette 5, Korea) was employed to reduce the grain size of aluminum powder. Aluminum powder (150 μm in size, 99.5% purity, supplied from Changsung Co. Ltd.) was charged into stainless steel bowls (500 mL) with 5-mm diameter stainless steel balls at a weight ratio of 1:15. Furthermore, 1wt% stearic acid (CH3[CH2]16COOH) was added as a process control agent to prevent excessive cold welding among the powders. The process cycle consists of 1-h of milling at a 200-RPM milling speed and a 2-h pause to cool down the powder. Four sets of aluminum powders were prepared by varying milling cycles (i.e., 0, 2, 7, and 12 cycles).

To obtain fully dense specimens, hot rolling was utilized. Before hot rolling, stearic acid was removed by heat-treating ball-milled powder at 500°C for 30 min. Then, the powder was packed in a one-end-sealed copper tube (outer diameter: 45 mm, length: 150 mm, and thickness: 1.2 mm) compacted with ~200 MPa of pressure at room temperature. Then, the other end of the copper tube was also sealed. The sample was heated to a predetermined temperature of 430°C; the sample required heating for ~40 min. Rolling was conducted with every 12% reduction. After 19 passes, the sample thickness was reduced to ~1.7 mm. The copper container was mechanically peeled off.

The grain size of the samples was analyzed using XRD (Rigaku, CN2301) with a CuKα radiation source (λ =1.5405 ?); high-resolution TEM (HRTEM, JEOL 2100FX) was used to check the grain size and morphology. XRD patterns were collected typically over 20-100° in 2θ. The XRD peak broadening was attributed to the refinement of grains.

HRTEM was used with an operating voltage of 200 keV. Thin specimens were prepared using a focused ion beam (FIB, DualBeam FIB Helios NanoLab 650, FEI Co., Ltd) for HRTEM observation. From the HRTEM images, the grain size was measured using the line intersect method [25].

Tensile tests were conducted using an Instron-type machine with a constant strain rate of 1×10^4 s^{-1}. For tests at room temperature, tensile specimens (thickness: 1 mm, gauge length: 25 mm, gauge width: 6 mm, and effective grip length: 160 mm for both upper and lower grips) were prepared according to ASTM standards. The specimens were subjected to the uniaxial tensile load in the rolling direction. After the tensile test, the morphologies of the fracture surfaces of the specimens were observed using a scanning electron microscope (SEM, JEOL, JSM 2001F, Japan). Specimens were attached to a carbon tape for SEM analysis.

3. Results and discussion

Fig. 1 shows the XRD results of the aluminum sheets after hot rolling. Compared to the pattern of the starting powders, the ball-milled samples showed broadened peaks, indicating that grain size is effectively reduced during ball milling. The recognition of grain growth occurred when the sample was exposed to high temperatures for a long period [24], and the condensed green compact was heated to the target temperature with a high average heating rate of ~20°C/min. It was then hot rolled at a relatively low temperature (i.e., 430°C, ~0.75 Tm, Tm is the melting point of aluminum), leading to negligible grain growth in the consolidated powder. The mean grain sizes of less ball-milled samples will be discussed later with TEM images. Interestingly, during hot rolling, a strong texture seemed to develop in the MC aluminum sheet, which was produced using the starting aluminum powder; the intensity of the peak corresponding to the (311) plane is the maximum of the MC aluminum sheet, whereas ball-milled specimens show typical maximum peak intensity at the lowest angle. In face-centered cubic (FCC) materials, textures develop in the rolling direction where tensile stress is applied to the materials. When the grain size is refined, however, the texture development becomes less significant.

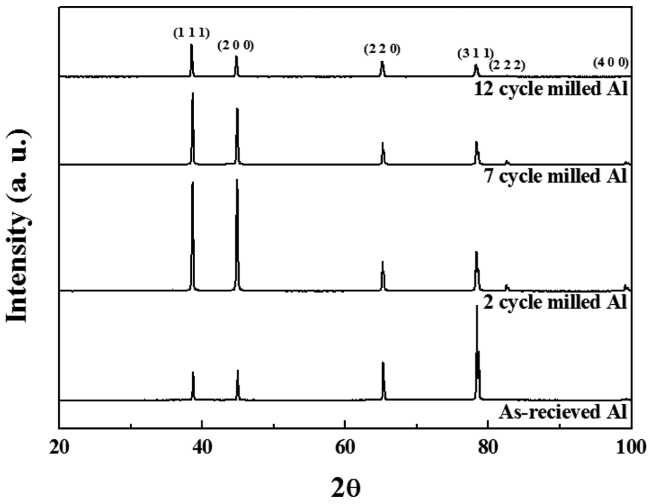

Fig. 1. XRD patterns of hot-rolled specimens, produced with starting and ball-milled aluminum powders

To confirm the grain sizes of the specimens, TEM analysis was performed. Fig. 2 shows TEM images of 2-cycle (Fig. 2. [a]), 7-cycle (Fig. 2. [b]), and 12-cycle (Fig. 2. [c]) milled specimens. Pores or other phases are not observed in these specimens. In Fig. 2 (a), despite a short milling time (2 h), many lattice dislocations were formed, and grain refinement occurred during the ball-milling process. In all hot-rolled specimens, regardless of grain size, long and thin columnar grains are observed to be arranged in the rolling direction. The average widths of the grains are measured using the line intersect method to approximately 750, 400, and 100 nm for 2-cycle (2-h-milling), 7-cycle (7-h-milling), and 12-cycle (12-h-milling) milled samples, respectively. Fig. 3 summarizes

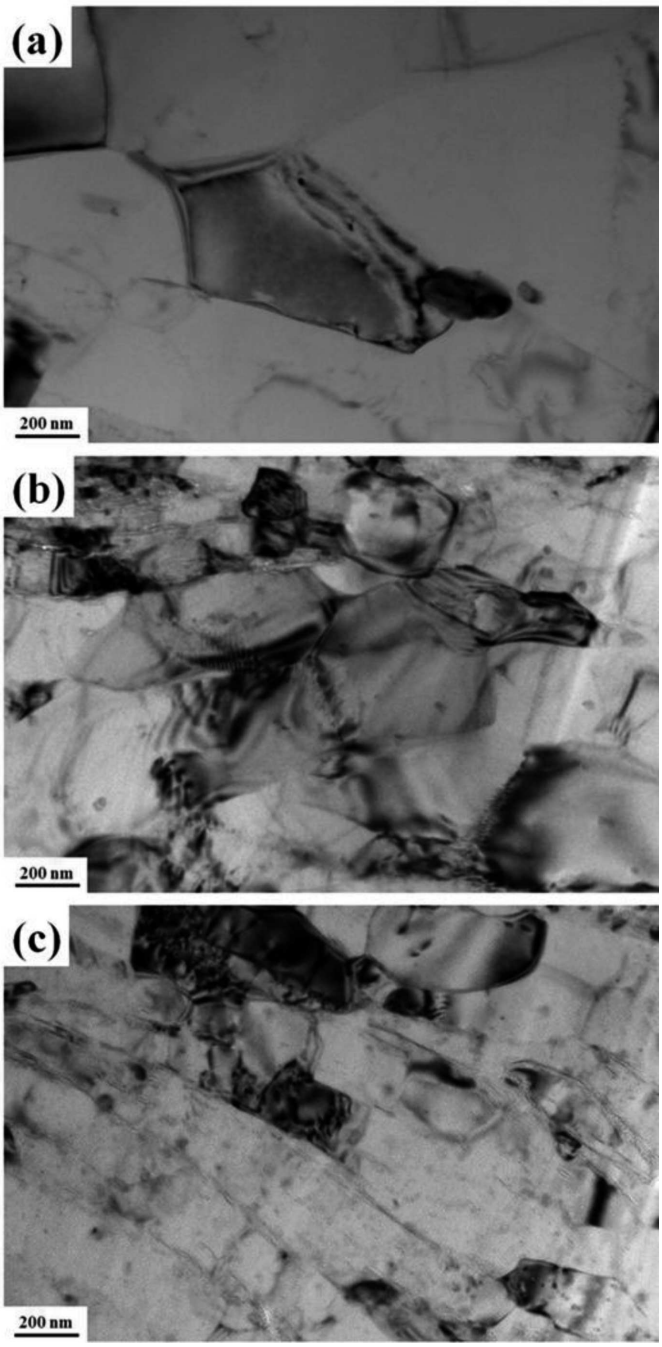

Fig. 2. TEM images of hot-rolled specimens, produced with a) 2-cycle-milled, b) 7-cycle-milled, and c) 12-cycle-milled powders

the relationship between the ball-milling cycle and the grain size. As shown, the grain size is found to be effectively reduced during ball milling. During the ball-milling process, powder is severely deformed by impact energy induced by stainless steel balls, and the grain size of the powder can be refined effectively via dislocation generation, formation of dislocation cells, and dynamic recrystallization. The grain boundaries in UFC metals, produced via SPD routes, generally seem to lose their sharpness and exhibit a "spotty" contrast, which indicates the presence of high-angle grain boundaries. Dislocations, trapped at the grain boundaries during SPD, may increase atomic mobility at the grain boundaries, resulting in rapid, discontinuous recrystallization. Hence, the cellular structures form a non-equilibrium grain boundary, shown with a spotty contrast [26]. Alternatively, the aluminum specimens used in the present study are more likely to show clear and sharp grain boundaries.

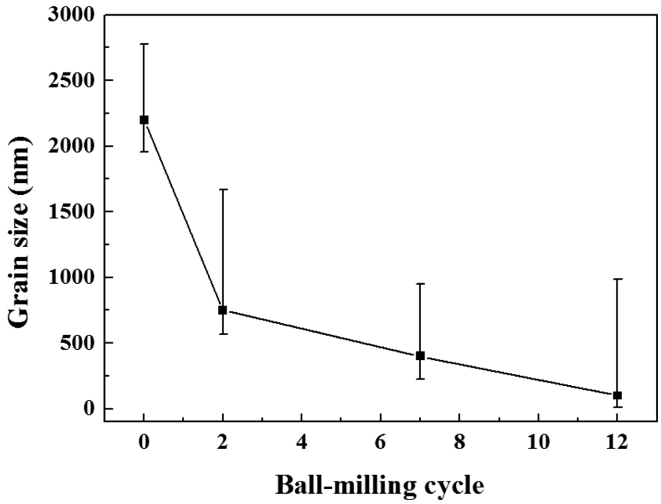

Fig. 3. Grain size as a function of the ball-milling cycle

Fig. 4 shows tensile stress-strain curves of hot-rolled specimens, fabricated using powders with different grain sizes (i.e., 100, 400, and 750 nm and 2.2 μm). A significant increase of flow stress is achieved as the grain size decreases. Aluminum with a grain size of 100 nm exhibits more than 3.5 times higher yield strength than that of the sample fabricated using the starting powders. Strain hardening tendency and ductility significantly decreases with decreasing grain sizes. The strain-hardening exponent (n) is obtained from the stress-strain curves in the plastic regime ($\sigma = k\varepsilon^n$, where k is constant). Compared to the value of MC aluminum (n = ~0.05), the n value of aluminum with a 100-nm grain size is around 3 times lower, as demonstrated in other NC metals [23]. The yield drops (as reported in UFC aluminum having undergone SPD [23]) are not observed in this study, possibly because of the lack of high-angle grain boundaries.

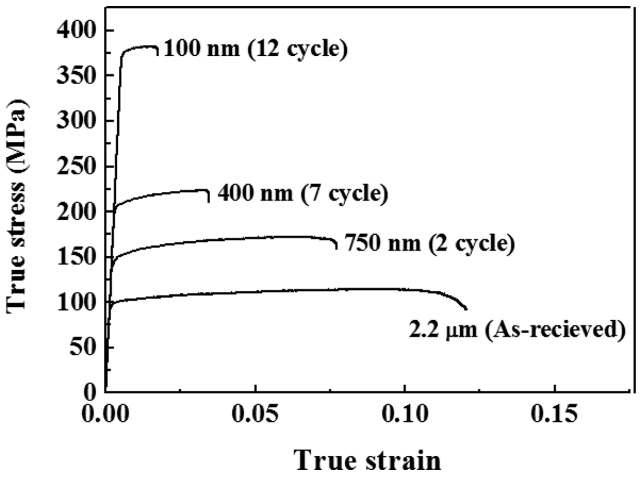

Fig. 4. Tensile stress-strain curves of hot-rolled specimens

As grain sizes decrease into the nano regime, forest dislocations–considered a main deformation mechanism in conventional metals–could hardly be observed because grain size is smaller than the dislocation mean free length. Thus, some transition in the deformation mechanism can occur based

on the length scale in grain size. In Fig. 5, yield stresses of aluminums, presented in this study and reported in other literatures [22, 24, 27-29], are plotted as a function of grain size ($d^{-1/2}$). Furthermore, calculated yield stresses based on the Hall-Petch equation [2], the deformation twin [13], the emission of partial and perfect dislocations [11], and grain boundary sliding [30] are also included. Based on the results, the deformation mode of aluminum at room temperature can be differentiated into three regions:

1. Region A: over 70 nm in grain size where the yield stress of aluminum follows the Hall-Petch relation;
2. Region B: grain size in the range of 70 nm down to around 40 nm where the yield stress of aluminum positively deviates from the Hall-Petch relation;
3. Region C: below 40 nm in grain size where the inverse Hall-Petch relation can be expected.

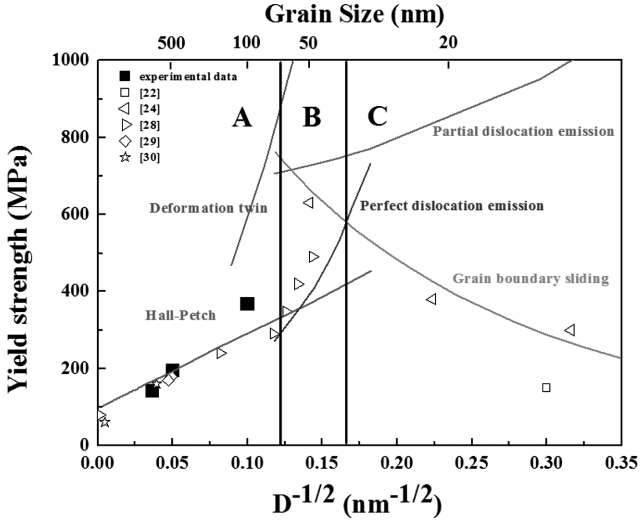

Fig. 5. A deformation map of aluminum with a wide grain size range

In Region A, as demonstrated by Hall-Petch strengthening behaviors in conventional metals, plasticity can be operated under lattice dislocation interactions with grain boundaries, and a consequence of forest dislocations leads to a high-strain hardening exponent and low strain-rate sensitivity [2, 3]. Our experimental data are put in this region.

In Region B, a unique deformation mechanism begins, attributed to a plastic deformation and intragranular slip involving the emission of dislocations from grain boundaries. For aluminum with high SFE, perfect dislocations have been preliminarily observed in MD simulations rather than partial dislocations or intrinsic stacking fault only; a leading Shockley partial dislocation emitted from grain boundaries travels only to a splitting distance. Subsequently, a trailing partial dislocation emitted from grain boundaries reacts with a leading partial dislocation to be a perfect dislocation [21, 22]. As noted in Fig. 5, in this region, the yield stress of NC aluminum [22, 24] does follow the dependence of d^{-1} rather than $d^{-1/2}$.

As the grain size is further reduced to below 40nm, the calculated resolved shear stress for a partial dislocation becomes lower than that of a perfect dislocation, as shown in Fig. 5. It will also increase in yield stress with the dependence of d^{-1}. The spherical grains around 10 nm, mostly located near large grains, experience much higher stress and a multi-stress state during deformation due to the constrained effects of larger grains. Therefore, sufficient stress could be provided to emit the dissociated dislocations. Furthermore, the stacking fault in aluminum could not easily pass through the whole grain if a trailing partial dislocation does not react with a leading partial dislocation to create a perfect dislocation. Liao et al. [21] have suggested the process of twin formation by dynamically overlapping two extended partial dislocations with stacking faults on adjacent slip planes for heavily deformed NC aluminum. In such cases, multiple twins are often located in the interior of the rains, which is different from conventional twins formed near the twinning plane when shear stress is applied. On the other hand, for NC copper having relatively lower SFE, deformation twins can be frequently observed in this region [31]. Thus, when the grain size is smaller than 70 nm, dislocations located at grain boundaries move to the opposite side along the slip plane without any dislocation pile-ups or tangles within the grains. That is, the emission of dislocations from grain boundaries during deformation could dynamically balance with an annihilation process at the grain boundaries.

As the grain size is further reduced (below ~40 nm, Region C), the deformation behavior could be additionally controlled in the form of atomic shuffling at the grain boundaries, leading to grain rotation or grain boundary sliding. That is, when the grain size is reduced comparable to the grain boundary width, the roughness of such slide planes decreases, and the stress required for grain boundary sliding decreases [28]. Therefore, together with the dislocation-mediated deformation of the emission of partial dislocations, grain boundary sliding simultaneously occurs in this region A. Portion of grain boundary sliding contributes to total deformation, which will increase as grain size is reduced, providing a decrease in yield stress as the grain size decreases. However, conventional grain boundary sliding in fine-grained aluminum at a high temperature could not occur, as shown in Fig. 5.

Fig. 6 shows SEM images of the fractured surface after tensile tests for samples, as prepared from starting (Fig, 6 [a]), 2-cycle-milled (Fig. 6 [b]), 7-cycle-milled (Fig. 6 [c]), and 12-cycle-milled aluminum powders (Fig. 6 [d]). All fracture surfaces exhibit dimples, evidencing ductile failure with the trans-granular fracture mode, although the dimple size decreases with decreasing grain sizes.

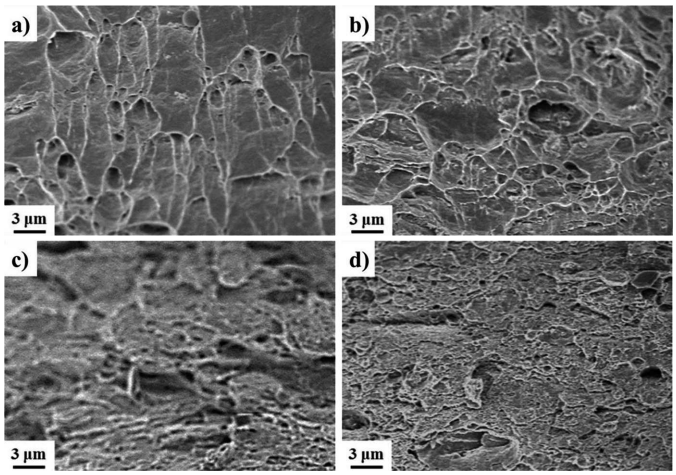

Fig. 6. SEM images of fracture surfaces after tensile tests

4. Conclusions

We fabricated an aluminum sheet with a variation of mean grain sizes from 2.2 μm down to 100 nm via mechanical milling and hot-rolling processes. Deformation behaviors of the specimens are characterized through conventional testing methods and compared with other literature data and theoretical models. In the grain size regime, the Hall-Petch strengthening behavior shown in conventional metals is observed as an evidence of lattice dislocation interactions with grain boundaries. Yield-drop phenomena, which has been reported in UFC aluminum having undergone SPD, is not monitored, possibly because of the lack of high-angle grain boundaries.

Acknowledgements

This work was supported by Basic Science Research Program (2009-0093814 and 2013-3005759) through the National Research Foundation of Korea (NRF) funded by the Ministry of Education, Science and Technology.

REFERENCES

[1] D. Wolf, V. Yamakov, S.R. Phillpot, A.K. Mukherjee, H. gleiter, Acta Mater. **53**, 1 (2005).
[2] P.G. Sanders, J.A. Eastman, J.R. Weertman, Acta Mater. **45**, 4019 (1997).
[3] G.W. Nieman, J.R. Weertman, R.W. Siegel, J Mater Res, **6**, 1012 (1991).
[4] J.S. Lee, J.C. Yun, J.P. Choi, G.Y. Lee, J. Kor. Powd. Met. Inst. **20**, 1 (2013).
[5] E.Y. Yoon, D.H. Lee, D.H. Ahn, H.J. Jeong, H.S. Kim, J. Kor. Powd. Met. Inst. **20**, 148 (2013).
[6] H.J. Hofler, R.S. Averback, Scripta Metall Mater. **24**, 2401 (1990).
[7] N.I. Noskova, Nanostruct. Mater. **9**, 505 (1997).
[8] D. Jia, Y.M. Wang, K.T. Ramesh, E. Ma, Y.T. Zhu, R.Z. Valiev, Appl Phys Lett. **79**, 611 (2001).
[9] S.X. McFadden, R.S. Mishra, R.Z. Valiev, A.P. Zhilyaev, A.K. Mukherjee, Nature, **398**, 684 (1998).
[10] H. Tanimoto, S. Sakai, H. Mizubayashi, Nanostruct. Mater. **12**, 751 (1999).
[11] R.J. Asaro, S. Suresh, Acta Mater. **53**, 3369 (2005).
[12] B. Cai, Q.P. Kong, L. Lu, K. Lu, Mater. Sci. Eng. A **286**, 188 (2000).
[13] M.W. Chen, E. Ma, K.J. Hemker, H.W. Sheng, Y.M. Wang, X.M. Cheng, Science **300**, 1275 (2003).
[14] H. Van Swygenhoven, P.M. Derlet, Phys. Rev. B **64**, 224105 (2001).
[15] H. Van Swygenhoven, P.M. Derlet, A. Hasnaoui, Phys. Rev. B **66**, 24101 (2002).
[16] V. Yamakov, D. Wolf, S.R. Phillpot, H. Gleiter, Acta Mater. **50**, 5005 (2002).
[17] V. Yamakov, D. Wolf, S.R. Phillpot, A.K. Mukherjee, H. Gleiter, Nat. Mater. **1**, 4347 (2004).
[18] M.A. Haque, M.T.A. Saif, Scripta Mater. **47**, 863 (2004).
[19] A. Hasnaoui, P.M. Derlet, H.V. Swygenhoven, Acta Mater. **52**, 2251 (2004).
[20] H.V. Swygenhoven, A. Caro, D. Farkas, Scripta Mater. **44**, 1513 (2001).
[21] X.Z. Liao, F. Zhou, E.J. Lavernia, D.W. He, Y.T. Zhu, Appl. Phys. Lett. **83**, 5062 (2003).
[22] H.J. Choi, S.W. Lee, J.S. Park, D.H. Bae, Mater. Trans. **50**, 640 (2009).
[23] N. Tsuji, Y. Ito, Y. Saito, Y. Minamino, Scripta Mater. **47**, 893 (2002).
[24] H.J. Choi, S.W. Lee, J.S. Park, D.H. Bae, Scripta Mater. **59**, 1132 (2008).
[25] H. Abrams, Metallography **4**, 59 (1971).
[26] C.Y. Yu, P.L. Sun, P.W. Kao, C.P. Chang, Mater. Sci. Eng. A **366**, 310 (2004).
[27] T.T. Sasaki, T. Mukai, K. Hono, Scripta Mater. **57**, 189 (2007).
[28] R.J. Asaro, P. Krysl, B. Kad, Philos. Mag. Lett. **83**, 733 (2003).
[29] A.S. Khan, Y.S. Suh, X. Chen, L. Takacs, H. Zhang, International Journal of Plasticity **22**, 195 (2006).
[30] H. Canrad, J. Narayan, Scripta Mater. **42**, 1025 (2000).
[31] J. Chen, L. Lu, K. Lu, Scripta Mater. **54**, 1913 (2005).

Received: 20 November 2014.